

Assessing the weather conditions for urban cyclists by spatially dense measurements with an agent-based approach

Amelie U. Schmitt^{1,2}  | Finn Burgemeister¹  | Henning Dorff¹  |
Tobias Finn³  | Akio Hansen¹  | Bastian Kirsch¹  | Ingo Lange¹  |
Jule Radtke¹  | Felix Ament¹ 

¹Meteorological Institute, Center for Earth System Research and Sustainability (CEN), Universität Hamburg, Hamburg, Germany

²Climate Service Center Germany (GERICS), Helmholtz-Zentrum Hereon, Hamburg, Germany

³CEREA, École des Ponts and EDF R&D, Île-de-France, France

Correspondence

Amelie U. Schmitt, Meteorological Institute, Center for Earth System Research and Sustainability (CEN), Universität Hamburg, Bundesstr. 55, 20146 Hamburg, Germany.
Email: amelie.schmitt@hereon.de

Funding information

Bundesministerium für Verkehr und Digitale Infrastruktur, Grant/Award Number: 4818DWDP1B; Deutsche Forschungsgemeinschaft, Grant/Award Number: 390683824

Abstract

Convincing commuters to use a bike is a timely contribution to reach sustainability goals. However, more than other modes of transportation, cycling is heavily influenced by the current meteorological conditions. In this study, we assess the weather conditions experienced on individual cycling routes through an urban environment and how weather observations and forecasts may give guidance to a better cycling experience. We introduce an agent-based model that simulates cycling trips in Hamburg, Germany, and a three-category traffic light scheme for precipitation, wind and temperature comfort. We use these tools to evaluate the cycling weather based on the commonly used single-station measurement approach versus spatially dense observations from an urban station network and radar measurements. Analysis of long-term data from a single station shows that most frequently discomfort is caused by temperature with a probability of 33%. Wind and precipitation discomfort occur only for about 5% of the rides. While temperature conditions can be well assessed by a single station, only one-third of critical precipitation events and less than 10% of critical wind events are captured. With perfect knowledge, temporal flexibility in start time of less than ± 30 min reduces the risk of getting wet by 50%. For precipitation, nowcasting is able to predict 30% of the critical events correctly, which is significantly better than model forecasts. Operational ensemble forecast provides satisfactory guidance concerning temperature; however, the limited predictability of precipitation and wind renders these forecasts only useful for riders with a high risk-awareness and small sensitivity to false alarms.

KEY WORDS

agent-based model, cycling, high-resolution measurements, urban mobility, weather forecasts, weather radar

This is an open access article under the terms of the [Creative Commons Attribution License](#), which permits use, distribution and reproduction in any medium, provided the original work is properly cited.

© 2023 The Authors. Meteorological Applications published by John Wiley & Sons Ltd on behalf of the Royal Meteorological Society.



1 | INTRODUCTION

New transportation concepts have emerged over the past years with the goal to reduce greenhouse gas emissions and to ensure more effective transportation within cities. Cycling routes are essential to these new concepts. More than other modes of transportation, cycling is heavily influenced by the current meteorological conditions (e.g., Brandenburg et al., 2007; Miranda-Moreno & Nosal, 2011; Tin Tin et al., 2012). Thomas et al. (2012) found that a combination of weather factors (temperature, duration of sunshine, precipitation and wind speed) could explain 80% of the observed variability in cycling volume in two cities in the Netherlands. Weather conditions can be quite variable even in the same city for a given time and may change within minutes, for example, during convective precipitation events. Therefore, better information about current and future weather events from meteorological measurements and forecasts can improve the cycling experience. In this study, we assess the weather conditions experienced on individual cycling routes through the urban area of Hamburg and how weather observations and forecasts may give guidance to a better cycling experience.

Previous studies often combined bicycle count data with measurements from weather stations to analyse the impact of weather conditions on cycling behaviour. Tin Tin et al. (2012) calculated linear regressions between bicycle counts in Auckland, New Zealand, and hourly measurements from a nearby weather station. They found that a 10% increase in cycling volume was related to either an increase in temperature of 4.4 K or in sunshine duration by 25 min or to a decrease in precipitation by about 1 mm or in wind gusts by 7.1 m/s. A similar result with a temperature increase of 4.0 K causing a 10% increase in cycling volume was found by Miranda-Moreno and Nosal (2011) for Montreal, Canada. Some studies also used survey data to assess the weather impact on transport choices (e.g., Helbich et al., 2014; Liu et al., 2014; Meng et al., 2016). Based on travel diaries and daily aggregated weather measurements for Rotterdam, the Netherlands, Böcker and Thorsson (2014) found negative relationships between bicycle use and both precipitation sum and wind speed. Temperature had a bell-shaped effect on cycling with an optimum on days with maximum air temperatures around 24°C. In a questionnaire for bicycle commuters in Melbourne, Australia, about 85% of people responded that rain had an impact on their decision to ride, while the impact was smaller for wind with 57% and temperature with only 34% (Nankervis, 1999). These studies identify precipitation, temperature and wind as the most relevant cycling weather parameters (see also Bean et al., 2021; Kruij

et al., 2021). Different studies suggested that precipitation also effects cycling choices with a time lag of a few hours (Miranda-Moreno & Nosal, 2011; Nosal & Miranda-Moreno, 2014; Zhao et al., 2018) and that commuters are more inclined to delay their trips to avoid bad weather compared to recreational cyclists (Morton, 2020).

A few studies also elaborated the impact of weather forecasts on cycling behaviour. In a survey conducted by Meng et al. (2016) in Singapore, more than 66% of people reported that they would change cycling plans if the weather forecast predicted rain. Kraemer et al. (2015) found that forecasted rain decreased the number of bicycle commuters in Washington, D.C., the United States, by 40%, while actual observed rain caused a decrease of only 28%. Wessel (2020) used bicycle counting stations from 37 cities in Germany together with television weather forecasts. They found that both actual and forecasted weather significantly influenced bicycle usage.

Most previous studies on the influence of weather on cycling used measurements from a single meteorological station or were even based on daily means of the considered meteorological variables. However, the weather experienced locally by individual cyclists may differ substantially due to both small-scale variability within the area of a city and rapid temporal evolution. This discrepancy between local perception and single point observation is an inherent reason for cyclists to complain regularly about weather observations and forecasts, even if they are scientifically without error. This study explores the potential of novel small-scale resolving observing systems to overcome this misconception by adequately capturing the local perception of cyclists. In particular, we analyse the benefits of a dense weather station network with kilometre-scale, along with precipitation radar data with a 100-m resolution—both providing minute-scale temporal resolution—for the Hamburg region in northern Germany. The results give guidance for the design of future urban observation systems that will be able to inform citizens about the individual perceived weather conditions. We also analyse how well weather forecasts are able to represent this variability and thus can serve to inform and predict cycling weather. More precisely, based on modern observations resolving urban weather variability in space and time, we aim to answer the following questions: (1) How often does a virtual typical commuter in an urban environment experience bad weather while cycling based on high-resolution meteorological observations? (2) Can smart cyclists, being informed by nowcasting and day-ahead forecast, effectively reduce the number of bad weather rides?

For this purpose, we introduce a three-category (green, yellow, red) traffic light scheme based on critical values for precipitation, wind speed and air temperature, which is then used as an indicator of cycling comfort. The data from weather stations, precipitation radars and

the COSMO-D2 model ensemble used in this study are described in Section 2. In Section 3, we derive the thresholds used for the traffic light scheme and introduce an agent-based model to simulate cycling trips of commuters in Hamburg. We assess the weather conditions for cyclists in Hamburg based on both a single station with long-term data (Section 4.1) and spatially dense data from precipitation radars and a network of more than 100 stations, which measured weather conditions in summer 2020 (Section 4.2). In Section 5, we analyse the potential of forecasts for improving the cycling experience. First, we evaluate how a flexible starting time of a cycling trip can reduce the chances of experiencing uncomfortable precipitation conditions (Section 5.1). As a second step, we analyse how well simple forecasts, such as persistence and nowcasting, and more complex numerical weather forecasts are able to capture the spatial and temporal variability of cycling comfort. Finally, we quantify the value of probabilistic ensemble forecasts for cyclists with different risk perceptions (Section 5.2).

2 | DATA

2.1 | Atmospheric measurements

In this study, we make use of numerous and various meteorological stations and instruments operated by our

institute (Figure 1), ranging from long-term single-point measurements ('Wettermast' and 'HUSCO') to a campaign setup during July and August 2020 of a spatially dense network of additional weather stations ('APOLLO' and 'WXT'). Precipitation is continuously monitored by a high-resolution X-band precipitation radar since 2021. In addition, we use the data of one C-band precipitation radar of the German weather service (DWD).

2.1.1 | Wettermast Hamburg (WMH)

The Wettermast Hamburg ('Hamburg Weather Mast') is a scientific measuring site operated by the Meteorological Institute of Universität Hamburg at the south-eastern outskirts of the city. It provides boundary layer tower measurements up to 280 m and additional ground-based instruments and standard meteorology. More information can be found in Brümmer et al. (2012). In this study, the Wettermast site plays the role of a local weather station, typically provided by national weather services as part of a greater network. Measurements at this site started in 1995, and different sensors have been added in later years. For the general analysis of cycling weather in this study, we only use precipitation, wind (10 m above ground) and temperature (2 m) data. Since the infrared rain detector was installed in 2006, we use 14 complete

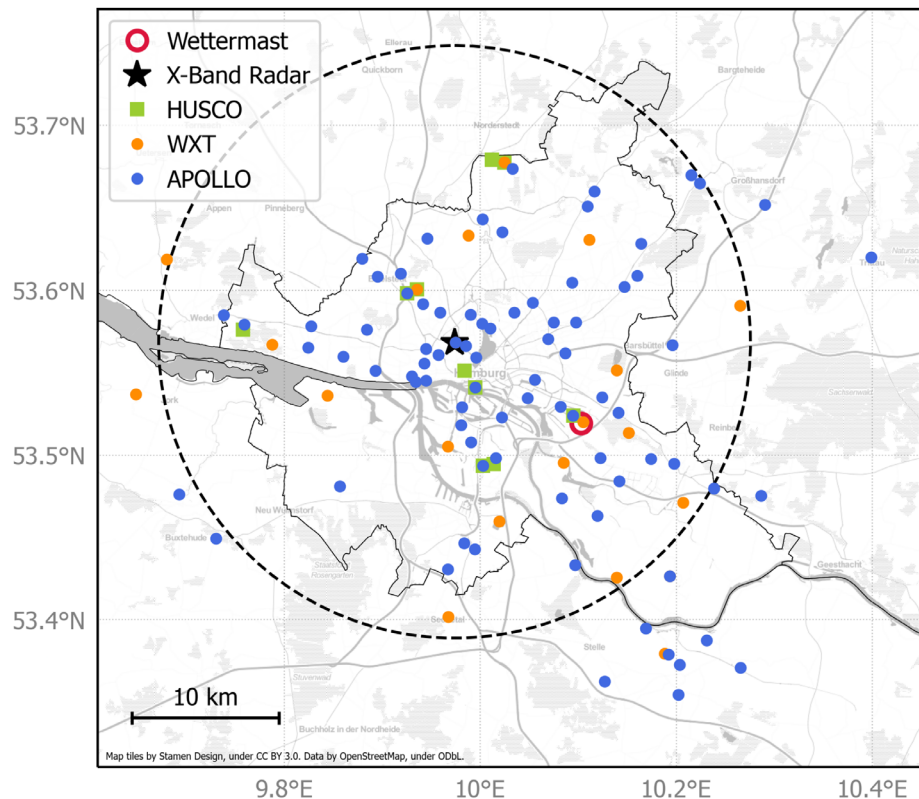


FIGURE 1 Overview of measurement locations in the greater area of Hamburg. More information about the station networks HUSCO, WXT and APOLLO are given in the text. The dashed circle line indicates the range of the X-band precipitation radar. The C-band radar of the DWD is located 50 km north of the city centre and scans the whole area.

years of data from 2007 to 2020 as a reference period. The temporal resolution of these data is 1 min.

Special processing was applied to the precipitation data. Due to the low resolution of the precipitation amount measured by the rain gauge (0.1 mm), for most weak precipitation events the time series alternates between values of 0.0 and 0.1 mm and, thus, is not suitable to represent a continuous precipitation event as desired in our agent-based model (see Section 3.2). For this purpose, we use additional data of a more sensitive infrared rain detector and distribute the precipitation amount values measured by the rain gauge to all minutes with a positive rain detection flag lying beforehand. This rain detector is in operation since mid-2006, which restricts our data set to the year 2007 and after. Additionally, Wettermast data are used to derive the temperature thresholds in Section 3.1.3. For this purpose, we use measurements of downward shortwave and longwave radiation, surface temperature, as well as air temperature and water vapour pressure at 2 m height.

2.1.2 | HUSCO stations

The Hamburg Urban Soil Climate Observatory (HUSCO) consists of 10 weather stations with focus on urban soil measurements across Hamburg. A typical HUSCO station is equipped with soil sensors and standard meteorology sensors providing data as 1-min averages. Some of these stations are arranged in pairs with a short distance to investigate the difference between urban and rural environments. Temperature sensors are mounted at 2 m height and wind sensors at 2.3 to 3.0 m height. Further details are described in Wiesner (2013). Only nine of the HUSCO stations provided wind measurements during the case study period in July and August 2020.

2.1.3 | APOLLO and WXT weather stations

Between June and August 2020, a dense network of 103 custom-built weather stations covered the greater area of Hamburg within the framework of the FESST@HH field experiment. The network featured 82 low-cost APOLLO (Autonomous cold POoL LOgger) stations that sampled air temperature and pressure at a resolution of 1 s and was primarily designed to capture rapid perturbation associated with frontal passages of convective cold pools. Furthermore, 21 WXT weather stations based on commercial sensors (Vaisala WXT 536) recorded air temperature, pressure, relative humidity, wind speed, wind direction and precipitation at a resolution of 10 s. All variables are sampled at a height of about 3 m above ground. A detailed description of the

measurement stations can be found in Kirsch et al. (2022). Here, we use air temperatures and wind from this data set (Kirsch et al., 2021) to get insights into the small-scale variability of meteorological parameters within the city.

2.1.4 | Radar

The precipitation variability experienced by bicycle commuters may be miscaptured by a few local rain gauge measurements. Therefore, we use spacious precipitation measurements estimated at different spatio-temporal scales by an X-band and a C-band weather radar. An operational, single-polarised X-band weather radar provides measurements within a 20-km scan radius around its location on the rooftop of the Meteorological Institute of Universität Hamburg in Hamburg's city centre (Figure 1). This local area weather radar operates at one elevation angle (3.5°) with a high temporal (30 s), range (60 m) and sampling (1°) resolution (Lengfeld et al., 2014), refining observations of the German nationwide C-band weather radars of the DWD. The DWD's C-band radar provides measurements within a 150 km radius and is located near Boostedt about 50 km north of Hamburg, thus scans the whole city area. We use the precipitation scan at the elevation angle 0.8° with a 5 min temporal, 250 m range and 1° sampling resolution.

The X-band precipitation rates (Burgemeister et al., 2022) are estimated from radar reflectivity values adjusted for several sources of radar-based errors, for example, the radar calibration, alignment, attenuation, noise and non-meteorological echoes (Burgemeister et al., 2023). Radar reflectivities of both radars were corrected for attenuation using the method of Jacobi and Heistermann (2016) implemented by Heistermann et al. (2013). The precipitation rates were retrieved from attenuation-corrected reflectivities using a power-law relationship between these two quantities ('Z-R relationship'), using the standard Marshall–Palmer relationship (Marshall et al., 1955).

2.1.5 | Data availability during case study period in July and August 2020

The availability of observation data typically depends on various external factors specific to the measurement instrument and variable. In case of the dense network of APOLLO and WXT stations (Section 2.1.3), the recording of measurement data was determined by the continuous power supply of batteries that needed to be changed on a regular basis. Due to limited human resources, this led to

some shutdowns of single stations after a certain period of time. The station network hence becomes partly coarser over the course of the period. For the example of temperature, Figure 2 depicts this temporal dependency on availability of measurement data. While HUSCO and Wettermast achieved entire data recording during the period, the WXT network was running during 95% of the time. For the APOLLOs, the decline in measurement data recording was strongest in the first 2 weeks. However, the data variability ranges between 87% and 95% and the availability is always higher than 80%, meaning that more than 60 APOLLO stations were running continuously. One WXT station was partly inactive causing a decrease for all three measurement quantities.

Throughout most of the analysis period, the radar systems were running smoothly. However, for days with significantly lower availability radar data are neglected, as indicated in grey. Analyses using precipitation data are limited to days where both X-band and C-band radars provide complete data.

2.2 | COSMO-D2 ensemble model data

The simulations of the operational Consortium for Small-scale Modelling (COSMO)-D2 model are performed every 3 h by the DWD, and its domain covers the whole area of Germany and parts of the neighbouring countries. The storm resolving simulations have a horizontal resolution of 2.2 km with hourly output values and a forecast horizon of 27 h per simulation. In this study, the weather forecast for the cycling decision on the following day is based on the 12-UTC run. Additionally, this study uses

the 20 ensemble members of the COSMO-D2 Ensemble Prediction System (EPS) to analyse the added value of a probabilistic forecast for cyclists. The different initial and boundary conditions of the ICON EUrope (ICOahedral Non hydrostatic) ensemble are used together with various model physics and soil moisture variations to set up the 20 different COSMO-D2 EPS members. Further information about the model, the ensemble and its physics can be found in Baldauf et al. (2016) and Baldauf et al. (2011).

3 | METHODS TO ASSESS URBAN CYCLING WEATHER

To evaluate the influence of meteorological conditions on the cycling experience, we use a three-category traffic light scheme for precipitation, wind and temperature. It identifies conditions, which are either nice/suitable (green), uncomfortable/barely suitable (yellow) or very uncomfortable/not suitable, including dangerous (red) (Section 3.1). To track and assess weather conditions experienced by virtual bicycle commuters, we introduce an agent-based Monte Carlo simulation using one bicycle counting station and proxy data for start and end points of the cycling trips (Section 3.2). The methods used to compare different data sets and to statistically evaluate the performance of forecasts are presented in Section 3.3.

3.1 | Classification of weather conditions

Previous studies have considered precipitation, wind and temperature as cycling-relevant weather parameters

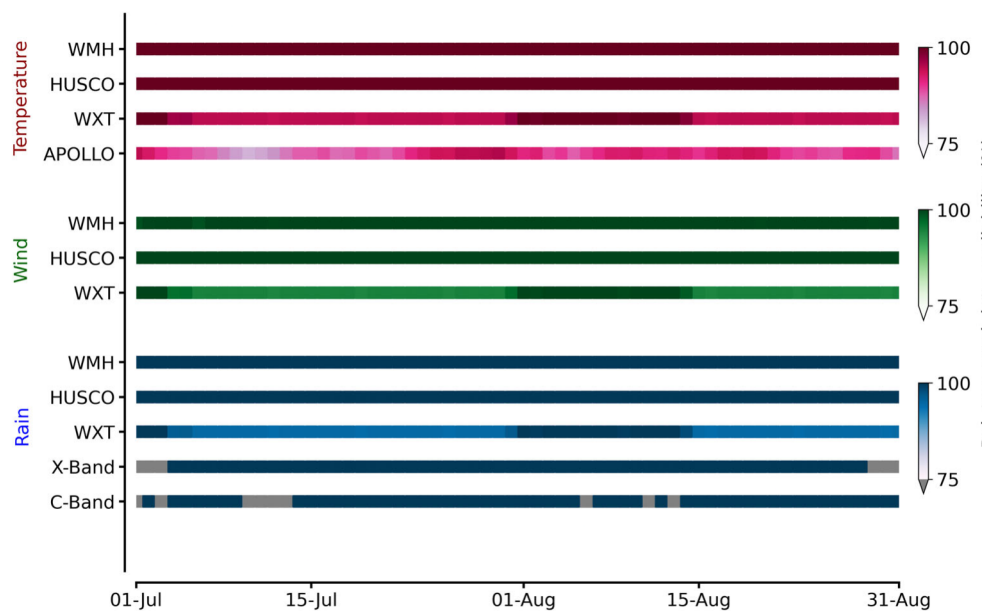


FIGURE 2 Relative temporal availability of device-specific station networks during the summer period of interest in 2020. Daily hundred percent availability is reached if all devices of one type are running continuously over the course of the day.

(e.g., Brandenburg et al., 2007; Goldmann & Wessel, 2020). Other weather factors influencing the cycling experience are, for example, low visibility during fog, icy roads or lightning during thunderstorms. Here, we focus on precipitation, wind and temperature only, since these quantities are widely available from measurements and model forecasts. A traffic light scheme for cycling comfort based on these three parameters is introduced in this section. The corresponding thresholds for each parameter are listed in Table 1 and described in more detail in the following sections.

3.1.1 | Precipitation thresholds

In the case of precipitation, we assume that cyclists collect water on their skin and clothes while riding. The more water they have collected, the more inconvenient they feel. A measure for this collected water amount should be the sum of the precipitation amounts given in mm for each minute of the trip. With that, we assume that a short but strong shower has the same effect as long moderate precipitation.

Starting from typical intensities of drizzle and rain that can be found in literature (Deutscher Wetterdienst, 2022b), and based on our own experiences on trips during extended rain events with known and constant intensity, we distinguish the three traffic lights empirically as follows: A precipitation sum below 0.1 mm means green (acc. to light drizzle for a typical trip duration), a moderate value from 0.1 to 0.5 mm means yellow (acc. to light rain for less than 10 min, e.g.), and more than 0.5 mm is red (Table 1).

3.1.2 | Wind thresholds

Common experience teaches us that wind has a significant impact on how comfortable a bike ride is. Two aspects must be taken into account: Moderate wind speeds have an influence on the power cyclists need to hold their own riding speed depending on the relative wind direction. Strong winds may be harmful either

directly to the cyclist's balance or indirectly regarding severe damages in the environment like breaking branches of trees.

The effect of strong winds is considered to be independent of wind and cycling directions. With respect to the DWD's warning categories (Deutscher Wetterdienst, 2022a), we choose 8 Beaufort (72 km/h) as a limit when cycling begins to be dangerous. This corresponds to warning level 2 (storm gusts). Since we only measure mean wind, we rescale this limit for wind gusts using a gust factor of 1.6. If the mean wind speed at 10 m height exceeds this condition (45 km/h), our traffic light turns red.

For cases without strong winds, the relative wind direction has to be taken into account. Schlichting and Nobbe (1983) derived a relationship for the power needed for an average cyclist to overcome the wind and rolling drag dependent on wind speed and direction. We consider sectors spanning 45° and ranging from headwind to tailwind and define thresholds for each. The traffic light changes to yellow (red) when the power needed to overcome the wind drag is twice (three times) the usual amount required in a windless situation. These thresholds are only considered if they are below the strong wind limit.

To calculate the specific limits, we assume a riding speed of 15 km/h. Since the formula of Schlichting and Nobbe (1983) considers the wind speed at the height of the cyclist, we first have to reduce our 10-m and 3-m wind speeds to 1 m height, approximating the centre of the body of a typical cyclist. Following the Klima-Michel model of Jendritzky (1990), this can be done by multiplying the 10-m wind by 0.67. To also convert measured 3-m winds to the height of the cyclists, we derive an additional scaling factor using Wettermast data. Based on wind speed measurements from 10 m and 3 m height, we obtain a factor of roughly 0.8 (not shown). The ratio of these two factors then yields a factor of 0.83 to convert 3-m winds to the height of the cyclist. Adjusting the strong-wind threshold to cyclist level then yields 30 km/h, accordingly.

All thresholds at cyclist's height can be found in Table 1. Note that only the thresholds for headwind and

Variable		Yellow	Red
Precipitation	Sum over trip	>0.1 mm	>0.5 mm
Wind (at cyclist level)	Headwind	>2.8 m/s (10.1 km/h)	>4.8 m/s (17.3 km/h)
	Cross headwind	>3.7 m/s (13.3 km/h)	>6.1 m/s (22.0 km/h)
	Strong winds		>8.3 m/s (30 km/h)
Temperature	Too cold	<5.5°C	<-3.1°C
	Too warm	>22.1°C	>24.4°C

TABLE 1 Traffic light thresholds for the three meteorological parameters affecting a cyclist riding at 15 km/h.

cross headwind are below the strong-wind threshold. In addition, cross-winds can also destabilise a bicycle. Studies indicate that for cross-wind speeds larger than the cycling speed, the side forces acting on the bicycle become larger than the drag forces (Kraemer et al., 2021). However, determining a critical wind speed for destabilising conditions would require extensive studies on actual cyclists or using wind tunnels, and thus, we decided to neglect this specific impact.

3.1.3 | Temperature thresholds

Weather stations and numerical weather prediction models typically provide air temperature as a variable. However, what matters more for the cycling experience is actually not the temperature but rather the thermal comfort of the cyclist (see, e.g., Brandenburg et al., 2007; Böcker & Thorsson, 2014). Besides air temperature, thermal comfort also depends on humidity, wind speed and radiation, as well as the clothing and physical activity of the considered individual (Jendritzky, 1990). A measure for the distribution of thermal comfort within a large group of people is the ‘predicted mean vote’ (PMV), which has been originally introduced by Fanger (1970) and ranges from -3 (very cold) to $+3$ (very warm). PMV can then be used to predict the number of dissatisfied people (PPD),

$$\text{PPD} = 100\% - 95\% \cdot \exp(-(0.03353 \cdot \text{PMV}^4 + 0.2179 \cdot \text{PMV}^2)). \quad (1)$$

Since the calculation of thermal comfort requires many variables that are not typically available from weather stations, we aim to find a relationship between PMV and air temperature, allowing us to derive thresholds for cycling comfort based on air temperature alone. We calculate PMV using the formulas in Jendritzky (1990) based on 14 years of Wettermast measurements (2007 to 2020). PMV is originally defined for pedestrians only and thus needs to be adjusted for the speed of the cyclist, which we assume to be 15 km/h in accordance with the agent-based cycling model in Section 3.2.

The results for PMV and PPD as a function of 2-m temperature are shown in Figure 3a,b. To obtain thresholds for our cycling traffic lights, we look at cold and warm discomforts (based on the sign of PMV) separately. We define the yellow (red) thresholds for more than 10% (50%) of people in discomfort. We then select all points within a $\pm 1\%$ interval of the 10 and 50% PPD thresholds and plot the corresponding 2-m temperatures as histograms and cumulative frequency distributions

(Figure 3c–e). By selecting a certain cumulative fraction (CF) threshold, we can then derive corresponding air temperature thresholds. An obvious choice would be the median and thus a CF threshold of 0.5. In Figure 4a, we present an example of classifications based on temperature thresholds derived using a CF value of 0.5 and compare them with classifications based on the PPD values via a contingency table. To assess the accuracy of our classifications, we calculate the total number of correct classifications by summing the values on the diagonal of the contingency table (highlighted in coloured boxes in Figure 4a). For a CF threshold of 0.5, this yields an accuracy of approximately 92.5%. We also tested whether an even better agreement could be obtained for other CF thresholds. Figure 4b illustrates that, for CF thresholds ranging from 0.45 to 0.75, the number of correct classifications always remains above 92%. The optimal agreement, reaching almost 93%, is achieved at a CF threshold of 0.65. Consequently, we have selected this CF threshold for calculating the temperature thresholds. The resulting four temperature thresholds can be found in Table 1.

We also tested whether the air temperature thresholds vary with season. However, we only found small variations over the course of the year, which can be neglected (not shown). In a second sensitivity study, we estimated the impact of the relative air speed (cycling speed combined with wind from different directions) on the thermal comfort. For a cycling speed of 15 km/h, a variation in the wind direction by 180° changes temperature thresholds by up to 0.2 K. However, the changes induced by varying the cycling speed by 5 km/h have a much larger impact and can change thresholds by more than 0.5 K. These results suggest that uncertainties caused by the choice of average cycling speed are much more important, and thus, the cycling direction is negligible for the derivation of temperature thresholds.

Different studies also focused on the impact of shading by buildings and trees on the experienced temperature stress (Fischereit, 2021; Hoffmann et al., 2018). We tested the impact of shading by recalculating the temperature thresholds using the method above and assuming that the direct solar radiation equals zero. As a result, warm thresholds increase by up to 2 K for shaded conditions and almost no impact is found for cold thresholds. However, since the overall classification of a cycling trip is based on the most extreme classification during the whole trip (see Section 3.2), our results would not change if we considered shading conditions for each street canyon. It is highly unlikely that a cycling trip would be shaded for the whole trip duration, and thus, we can neglect the shading impact on temperature thresholds.

We want to stress that the thresholds in Table 1 are only valid for a cyclist moving at 15 km/h in a region

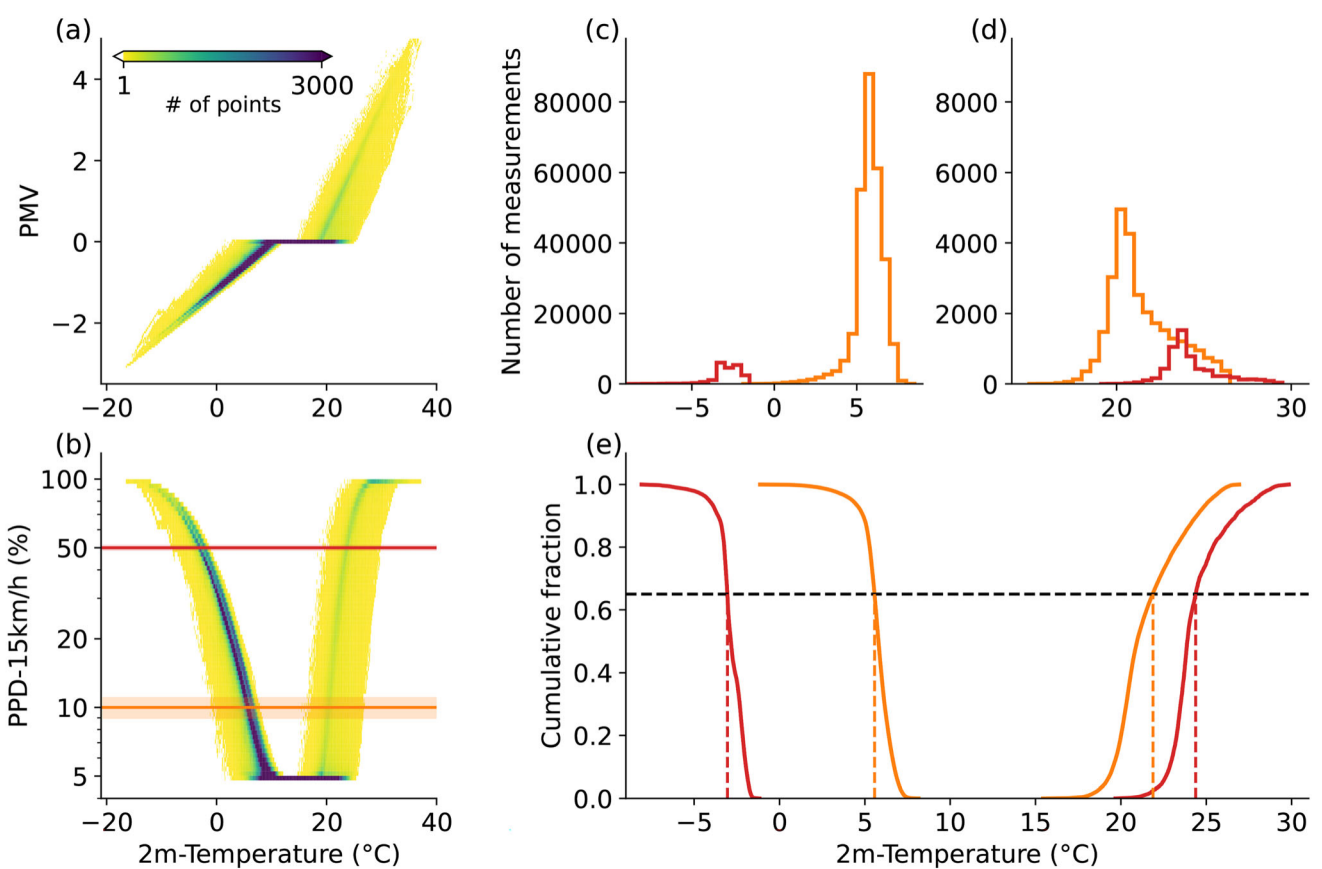


FIGURE 3 (a) Predicted mean vote (PMV) and (b) number of dissatisfied people (PPD) as a function of 2-m temperature at the Wettermast for the years 2007–2020. Red and yellow horizontal lines indicate the PPD thresholds, which are used to determine temperature thresholds. Histograms (c, d) and cumulative fractions (e) of the temperature values within the considered red and yellow PPD bins in panel (b). The horizontal dashed lines mark the optimised threshold for the cumulative fractions and the red and yellow vertical lines the corresponding temperature thresholds for too cold and too warm conditions.

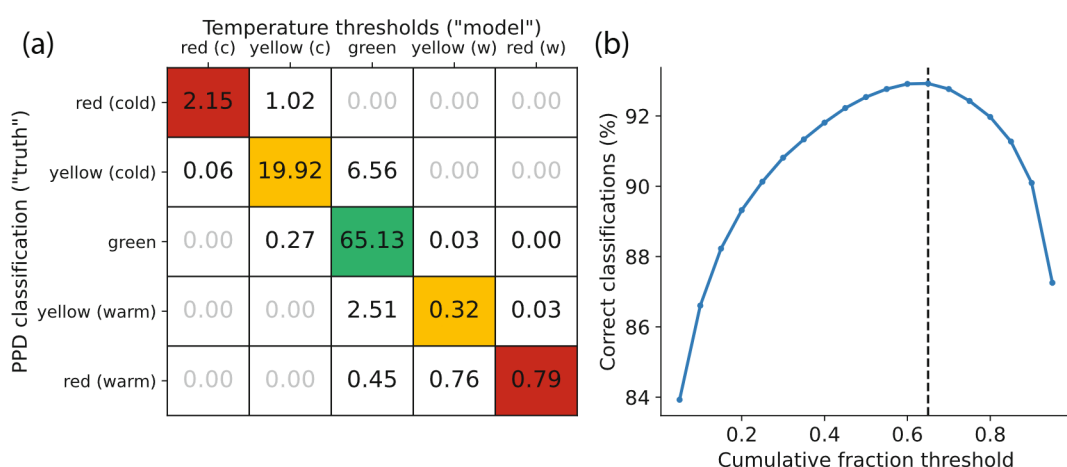


FIGURE 4 (a) Contingency table comparing temperature classifications based on PDD values and on the derived temperature thresholds using the median (0.5) as cumulative fraction threshold. The coloured boxes on the diagonal represent correct classifications. (b) Fraction of correct classifications for different cumulative fraction thresholds. The dashed line indicates the final choice of 0.65.

with similar overall climate as measured by the Wettermast, that is, the larger Hamburg region. For other local climates, new thresholds can be determined using our method described in this section.

3.2 | Agent-based model for bicycle commuting

The availability of bicycle counting stations or assessments of bicycle commuter flows in urban environments are limited. To, nonetheless, assess cycling weather that accounts for the individuality and diversity of cycling trips and thus the weather conditions experienced, we develop a novel agent-based Monte Carlo model that simulates cycling trips of commuters in Hamburg.

Each evaluation day, 10,000 virtual cyclists are propagated in space within the urban area of Hamburg from given start to end points along coordinates of routes. The cycling routes are based on OpenStreetMap bike network data and created with the python package OSMnx (Boeing, 2017). The start and end points are randomly drawn from a discretised latitude–longitude grid at a 100-m scale based on trip production and attraction rates derived from proxy data.

The trip production rate is proportional to the population in a district (Yang et al., 2014). We use as proxy data for the trip production the spatial distribution of the number of inhabitants raised by German authorities in 2011 (Statistikamt Nord, 2011) provided with a resolution of 100 m. More recent data with such a high spatial resolution are not available, only on district level from 2019 (Statistikamt Nord, 2020). By comparing the number of inhabitants per district from both data sets, we obtain a multiplicative correction factor, which is then used to update the population distribution. The lower limit of population is 500 inhabitants per grid point to avoid outliers. Remapped on the latitude–longitude grid, the ratio of inhabitants per grid point to the sum of all inhabitants of Hamburg results in the probability of a starting point.

The trip attraction rate is correlated to the density of points of interest on a district level (Yang et al., 2014). We retrieve the trip attraction rates based on land for industrial or commercial purpose given in Hamburg's land-use plan (Freie und Hansestadt Hamburg, 2018b). We assign different weights for multiple land-use categories, like industrial and commercial (1.0), mixed (0.6), airport and harbour (0.4), or residential (0.1) areas, which are based on the expected number of workplaces per area. Discretised on the latitude–longitude grid, the ratio of weight per grid point to the sum of weights describes the probability of an end point.

The bicycle commuter flows are modelled following a gravity approach (e.g., Balcan et al., 2009; Lenormand et al., 2016; Yang et al., 2014). The gravity model assumes that the probability of commuting w_{ij} between two locations, \mathbf{x}_i and \mathbf{x}_j , is proportional to the product of the trip production rate p_i and trip attraction rate a_j , and inversely proportional to the travel costs,

$$w_{ij} \propto p_i a_j f(d_{ij}), \quad (2)$$

with their distance $d_{ij} = \|\mathbf{x}_i - \mathbf{x}_j\|_2$ and $f(d_{ij})$ being a function describing the travel costs. The travel costs are modelled with an exponential distance decay function:

$$f(d_{ij}) = \exp\left(-\frac{1}{\tau}d_{ij}\right), \quad (3)$$

with the length-scale τ .

With this gravity model, we create bicycle routes in two steps. First, we sample the end point of a route, $\mathbf{x}_{j,\text{end}}$. Second, we sample the start point, $\mathbf{x}_{i,\text{start}}$, using the probability π_{ij} of the i -th grid point being the start point,

$$\pi_{ij} = \frac{f(d_{ij})p_i}{\sum_k f(d_{kj})p_k}, \quad (4)$$

with its trip production rate p_i . To retrieve a realistic bicycle route length distribution, we assume the empirical length-scale of $\tau = 2000$ m and limit the travel distance to a minimum of 150 m; below this threshold, we assume walking distance. The mode of the resulting bicycle route length distribution is 3250 m, and the median is 5665 m (not shown); therefore, the distribution has a reasonable range as shown by surveys (e.g., de Haas & Hamersma, 2020; Nobis, 2019; Schantz, 2017; Schneider et al., 2022).

Then, to each obtained route, a starting time is assigned, which is based on an average diurnal cycle derived from hourly bicycle counter data (Freie und Hansestadt Hamburg, 2018a) from 8 October 2014 to 22 November 2020. The counting station is located close to the city centre of Hamburg (Figure 5) and is highly frequented by commuters during weekdays and by recreational cyclists mostly during weekends and holidays. Daily cycles of bicycle counts for weekdays typically show two maxima in the morning and in the afternoon for utilitarian use and, for weekends, a single maximum in the afternoon for recreational use (not shown). Since the focus of this study is on bicycle commuters, we only consider bicycle counts from weekdays. A mixture of two Gaussian functions is fitted to

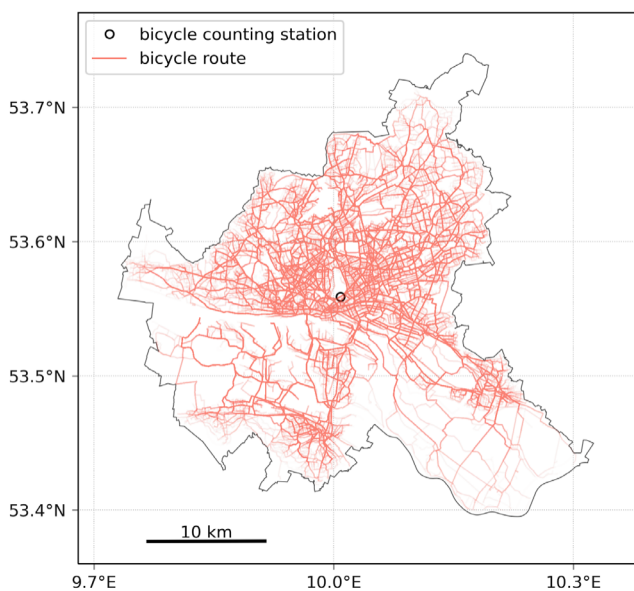


FIGURE 5 62,000 randomly drawn bicycle routes of the 620,000 bicycle routes used during the case study period in July and August 2020. The darkness of the bicycle routes scales with the number of bicycle routes passing the location. The location of the bicycle counting station is indicated with a circle.

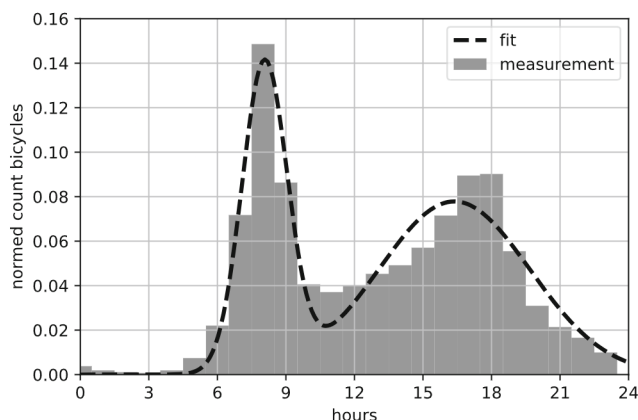


FIGURE 6 Normed median count of bicycles on weekdays for all seasons, including the fitted starting probability at local time. Based on hourly bicycle counter data at one highly frequented bike lane in the centre of Hamburg from 8 October 2014 to 22 November 2020.

the daily cycle of bicycle counts (Figure 6). We use data from the whole period since the seasonal changes of the overall shape of the fitted functions are small (not shown). The cycling routes are discretised on a 1-s temporal resolution with the assumption of a constant speed of 15 km h^{-1} .

We evaluate the cyclists' weather conditions for 10,000 randomly drawn bicycle commuters for every day within the period from July to August 2020

(Figure 5). The weather data (Section 2) are spatio-temporally assigned to the route coordinates using nearest-neighbour interpolation. Finally, we apply the meteorological traffic lights and the corresponding thresholds introduced in Section 3.1. A route is classified as red if it contains at least one red segment, as yellow if it contains yellow but no red segments, and as green if every segment is classified as green.

We introduce the agent-based model to include spatial variability of weather conditions in the statistical analysis of cycling comfort. It is a first approach constrained by realistic conditions, such as official bike routes and measured temporal cyclist patterns. To obtain an even more realistic distribution of cycling trips, future studies could make use of the constantly growing databases of cyclist traffic volumes based on Global Positioning System (GPS) positions from smartphones (e.g., Freie und Hansestadt Hamburg, 2022; Lißner et al., 2018). Our approach defines fixed routes and starting times and assesses the cycling comfort for each cycling trip. Future analyses could also enable decision-making of the cyclists by allowing them to change the route or the mode of transportation. Such an agent-based modelling framework has been introduced and tested in the Hamburg region by Yang et al. (2018), for example, who simulated the exposure of commuters to environmental stresses.

3.3 | Evaluation of forecasts

3.3.1 | Skill scores

To assess the potential of forecasts in reducing bad weather rides and to evaluate how different the cycling weather is assessed by spatially dense measurements compared to a single station, we use the Critical Success Index (CSI, or also Threat Score) and Equitable Threat Score (ETS or Gilbert score). Both scores only take into account critical events, that is trips with red or yellow weather conditions. Correct negatives (green weather conditions) are not considered. Speaking in terms of forecast potential, only times with observed or forecasted critical weather conditions are considered. The CSI then measures the fraction of correctly classified events (hits) out of all critical events (hits + misses + falsealarms). The ETS additionally takes into account the climatological frequency of an event; that is, some hits can occur purely due to random chance ($\text{hits}_{\text{random}}$). It measures the fraction of correctly classified events adjusted for chance ($\text{hits} - \text{hits}_{\text{random}}$) out of all critical events (hits + misses + falsealarms - $\text{hits}_{\text{random}}$). Both CSI and ETS range from 0 to 100%, where 100% represents a perfect forecast.

3.3.2 | Frustration reduction

The added value of the COSMO-D2 ensemble forecasts for cyclists is examined by calculating the frustration reduction potential to not experience bad weather or miss a ride during good weather. The calculation is based on the relative economic value (Richardson, 2000). In principle, there are two groups of cyclists for which individual risk perception factors R_{fact} are defined. The first group is more sensitive to bad weather conditions ($R_{\text{fact}} > 1$) and rates with a risk perception factor of one to four, for example, one ride with bad weather like missing four rides with good weather. The second group has the opposite risk perception ($R_{\text{fact}} < 1$) and is more sensitive to missed rides in good weather. If there is a perfect forecast, there will be no frustration. In contrast, if there is no forecast at all, always accepting bad weather or missing rides, the frustration will be

$$F_{\text{no}} = \min((1 - p_{\text{clim}})R_{\text{fact}}, p_{\text{clim}}), \quad (5)$$

with p_{clim} being the climatological probability of experiencing bad weather. Furthermore, the contingency table with hits, falsealarms, missedevents and correctnegatives is calculated and normalised. Based on the contingency table, the experienced frustration is

$$F = \text{false alarms} \cdot R_{\text{fact}} + \text{missed events}. \quad (6)$$

The potential to reduce the frustration for cyclists by using forecasts is derived by

$$F_{\text{red}} = \frac{F_{\text{no}} - F}{F_{\text{no}}}, \quad (7)$$

which points out the forecast skill and is used for the analysis of the COSMO-D2 ensemble.

4 | WEATHER CONDITIONS FOR CYCLISTS IN HAMBURG

By applying our traffic light evaluation method (Section 3.1), we investigate how favourable the meteorological conditions for cyclists in Hamburg are. We first conduct a multi-year analysis using the single-station data of Wettermast Hamburg. Based on this, we further assess how representative single-point measurements are to describe prevailing urban meteorological conditions for cyclists and compare them to a spatially dense measurement coverage. For this, we make use of our agent-based model with cyclists on 10,000 routes (Section 3.2).

4.1 | Single-station-based assessment

First, the cycling weather conditions obtained from single-station measurement data are investigated in more detail by a multi-year analysis. For simplicity, we do not use the routes from the agent-based model for this first analysis but only take into account the bimodal distribution of the daily traffic volume (Figure 6). For precipitation, we assume a trip duration of 30 min, for wind, we use 10-min averages and wind coming from a random direction, and for temperature, we just consider the 1-min values.

Following the method of Section 3.1, Figure 7 depicts our traffic light scheme applied to the 14-year data set from the Wettermast site. According to our considered thresholds (Section 3.1), cycling weather in Hamburg is quite favourable, on average, as the traffic light shows the green signal for at least two-thirds of the trips for each meteorological variable. In particular, precipitation and wind lead to cycling discomfort for less than 5%. While precipitation events cause considerable discomfort in about 2% of the trips, wind has a minor impact with 0.2%. Remarkably, temperature is the most dominant meteorological factor for cyclists' discomfort, causing unfavourable cycling conditions for one-third of all trips.

To elaborate statistics of cycling weather conditions on seasonal scale therefrom, Figure 8 shows 14-year monthly averages of cycling conditions based on the Wettermast single-station data set. Although the city of Hamburg is notorious for its rainy weather, our results suggest that dry cycling is actually possible for more than 90% of the time every single month. Seasonal variability is small, but higher percentages of very uncomfortable cycling conditions in June/July and broader transition zones (yellow) in winter seasons somewhat represent the increase of convective showers in summer and frequent light precipitation in winter.

Strong-wind events preventing comfortable cycling remain rare throughout the year. Every month shows very uncomfortable cycling conditions for less than 1% of the trips. Compared to that, the yellow transition zone is relatively broad, characterising almost 5% of the trips for the entire year with roughly 7.5% in the spring season (March, April, May) and less than 2.5% during mid- and late-summer.

Besides the fact that temperature affects cyclists the strongest on yearly average, thermal cycling conditions show the largest variability on seasonal scale (Figure 8c). Severe cycling discomfort occurs most frequently in the summer season (June, July, August) with warm discomfort for more than 12% of the trips, while transition seasons are most attractive for cycling in terms of heat. Remarkably, while up to 10% of the trips in January and

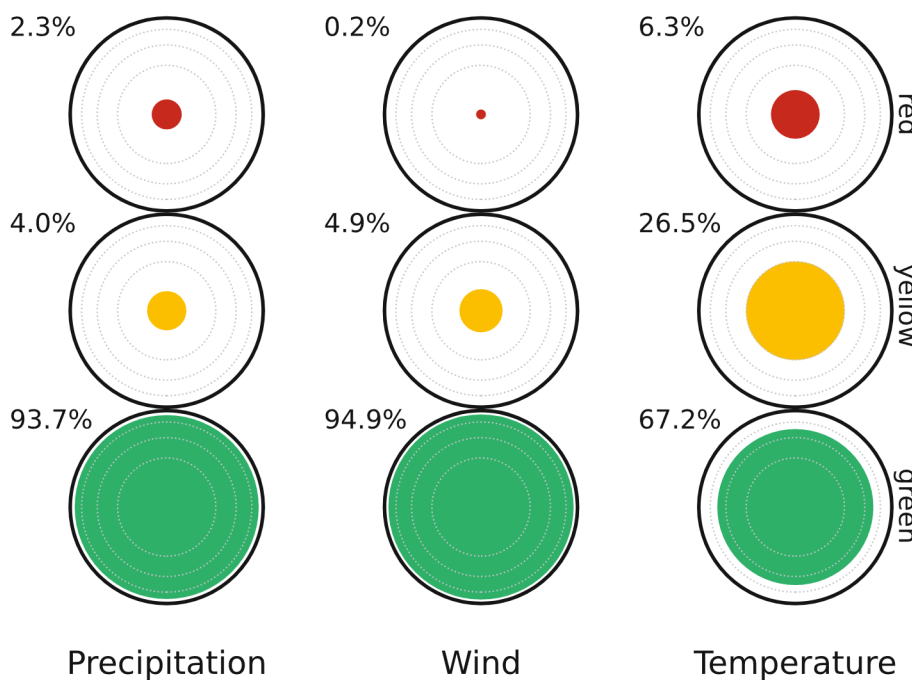


FIGURE 7 Traffic light scheme of cycling-relevant weather parameters based on thresholds specified in Section 3. The coloured areas scale with the frequency of occurrence, as given in percentages in the upper left. Grey dashed contour lines indicate frequencies of 25%, 50% and 75%, respectively. Over the long-term period, precipitation values were not available for 0.7%, wind for 0.8% and temperature for 0.6%.

December also contain strongly unfavourable (cold) cycling conditions, most of the trips are here dominated by slight cycling discomfort described by our transition zone (yellow). Altogether, only 30% of the trips in January and February are certainly suitable for cycling. It is also notable that during April, it is possible to experience both cold and warm thermal discomfort.

As noted above, these results account for the average distribution of cycling trips during weekdays. We analysed the impact of this assumption by comparing the results to those without any weighting (black lines in Figure 8). The differences for precipitation and wind are generally small, while notable differences occur for temperature in the summer months. The afternoon peak of the bimodal distribution of the cycling frequency coincides with those hours during which daily maximum temperatures are typically observed in summer. Consequently, the weighted results have a larger fraction of warm discomfort.

Our results are in line with those of Goldmann and Wessel (2020) and particularly with Brandenburg et al. (2007) analysing cycling weather in Vienna (Austria) using single-station data, which similarly showed that cycling conditions are dominated by the thermal comfort. Although most studies refer to single-station based analyses for a specific urban area, their representativeness when describing decakilometre scales, as common for large cities, remains limited. Subsequent studies dealing more with the spatial variability hence remain crucial.

4.2 | Assessment with spatially dense measurements

We now investigate how well weather conditions for cyclists in Hamburg can actually be assessed by a single-point measurement station, as carried out in the previous section, compared to spatially dense measurements. To do so, we turn to a case study period spanning July to August 2020. During this period, the FESST@HH measurement campaign took place (Kirsch et al., 2021), together with existing stations, providing unique dense measurements of precipitation, wind and temperature over the area of Hamburg (see Section 2.1). We combine all available measurements to data sets with different spatial resolution, using the data set with the highest spatial resolution as our baseline data set. For each data set, we apply the agent-based model described in Section 3.2 and classify each trip using our traffic light thresholds. See Table 2 for an overview of the different data sets and the corresponding relative fractions of green, yellow and red cycling trips during the study period. Since we only consider the summer season, critical temperature conditions are only related to warm discomfort. In summer, we also mainly observe convective precipitation and fewer strong-wind conditions than in the other seasons (see Figure 8). As seasonal changes, however, are small, we expect our overall conclusions to be valid also in other seasons.

On average, the differences between the data sets with coarser and denser resolutions are below 2%. However, for a total number of critical trips (red or yellow) in

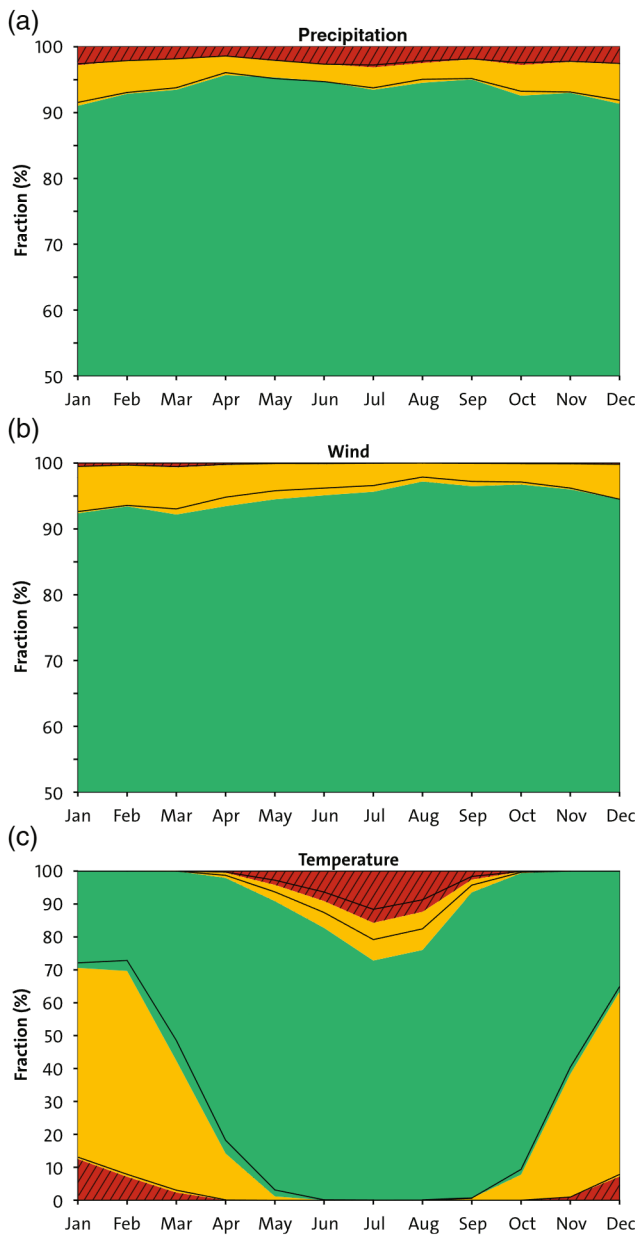


FIGURE 8 Seasonal variability of cycling weather conditions for (a) precipitation, (b) wind and (c) temperature. Red conditions (very uncomfortable) are represented by the dashed area at the top, followed by yellow (uncomfortable) and green (nice). For temperature, yellow and red areas at the bottom of the figure correspond to cold discomfort and at the top to warm discomfort. Long-term monthly average values of frequencies of occurrence for weather conditions based on Wettermast data from 2007 to 2020. Filled contours show the values weighted for the cycling behaviour Gauss function (see Section 3.2). Black lines do not consider any daily weighting, showing the statistics for the entire data set. Based on a 30-min trip duration for precipitation, 10-min averaged values of wind speed with random directions, and 1-min values for temperature.

the order of 2 to 4% (wind) to 26% (temperature), such differences are not negligible. For the further analysis, we now compare the classification of each route for different

TABLE 2 Fractions of green, yellow and red trips during the case study period in July and August 2020.

Data set	Green	Yellow	Red
<i>Precipitation</i>			
X-band radar*	93.8%	4.3%	1.9%
C-band radar	92.6%	4.9%	2.5%
WMH	94.0%	3.5%	2.5%
<i>Wind</i>			
WMH-HUSCO-WXT*	98.0%	1.7%	0.3%
WMH	96.0%	3.9%	0.2%
<i>Temperature</i>			
WMH-HUSCO-WXT-APOLLO*	73.8%	8.5%	17.7%
WMH-HUSCO-WXT	74.0%	8.3%	17.6%
WMH	74.5%	8.3%	17.3%

Note: The asterisks mark the baseline data sets for each variable.

data sets and compute the CSI (see Section 3.3.1). We use the baseline data set as a reference to compare to coarser spatial measurements and ultimately the single-point measurements at Wettermast.

Figure 9 shows that for precipitation, the single-point measurements at Wettermast are only moderately representative. About 35% of the critical precipitation conditions are classified correctly by the single-point measurements. The C-band radar classifies around 65% of the critical precipitation conditions correctly. Wind conditions can be least well classified by single-point measurements. Only 7.2% of the critical wind conditions are correctly classified by the Wettermast. In contrast, single-point measurements can well distinguish whether temperature conditions are suitable for cyclists. Nearly 90% of the red and 80% of the red or yellow events are classified correctly by the Wettermast. Spatial but still coarse measurements (WMH-HUSCO-WXT) provide little added value compared to the Wettermast. To exclude the effect of correct classifications by chance, we also calculated ETS values, which are up to 6% smaller than the CSI values but do not change the overall picture of the results.

It is remarkable that for precipitation and, to a certain extent, also for wind, CSI values are much lower than would be expected from the results in Table 2. While the Wettermast captures the average number of critical precipitation trips even better than the C-band radar, the CSI value reveals that this good agreement is only valid on average and not locally for each trip. This means that a single station is able to reproduce the overall amount of precipitation and wind gusts in the considered region but does not get the right timing, which is what we would

expect for highly variable conditions, for example, within rain showers.

How representative a single-station measurement is depends most likely also on the distance of the cyclist to the measurement location. Accordingly, we calculate the mean distance of each trip to the Wettermast location and calculate separate CSI values for distance bins of 2 km. The strongest change with distance is observed for precipitation. Figure 10 shows that the CSI drops from 40% at 5 km distance to 30% at about 20 km distance. A dependence on distance is not discernible for wind. For temperature, the CSI also decreases with increasing distance but very slowly. At 20 km distance, critical temperature events can still be well classified by the Wettermast with 75% for yellow and red and 85% for red events.

5 | FORECAST POTENTIAL

Weather forecasts of different types and complexity can help cyclists to improve their cycling experience by scheduling trips in comfortable weather conditions. The forecasting of weather has a long history and various methods have been developed. The common cyclist is confronted with a large set of forecast types and experiences, which are used in the upcoming subsections to assess their added value for the planning of cycling trips.

5.1 | Perfect forecast

In case of precipitation, the decision-making based on even perfect forecasts will not prevent cyclists from

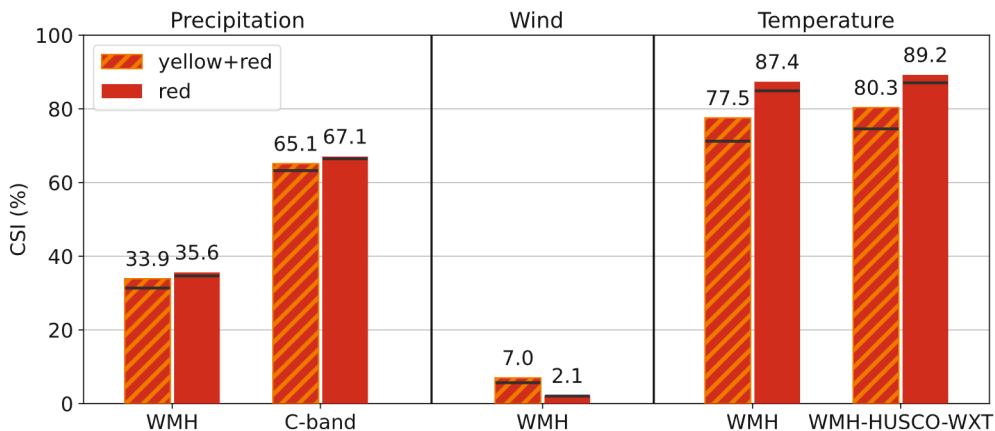


FIGURE 9 Critical Success Index (CSI) between the data sets denoted at the *x*-axis and the corresponding baseline data sets, which are X-band radar for precipitation, WMH-HUSCO-WXT for wind and WMH-HUSCO-WXT-APOULLO for temperature. Red bars consider only trips classified as red, and striped bars consider both red and yellow trips. The black horizontal lines indicate the corresponding ETS values.

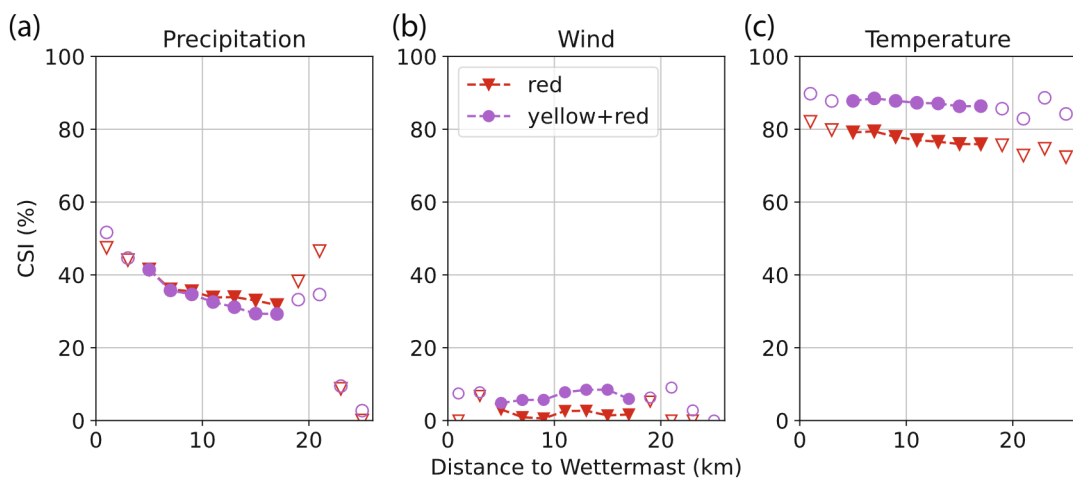


FIGURE 10 Critical Success Index between the baseline data sets (see Table 2) and the Wettermast data as a function of average distance of the trip to the Wettermast for precipitation (a), wind (b) and temperature (c). Empty symbols denote bins containing less than 5% of all trips.

getting wet, because staying at home is not an option for most commuters. However, many companies may provide flexible working hours, allowing the employees to start their commute in a certain time slot as they wish. In this section, we analyse how such a flexible starting time can reduce the chance of getting wet. For this purpose, we consider both data from a single station (WMH) but for multiple years from 2007 to 2020 as well as high-resolution X-band radar data for our study period in summer 2020.

For the single-station data, we assume that a cyclist has to do a 30-min trip around 9 a.m. but can freely choose the starting time within a window of $\pm\Delta t$, for example, $\Delta t = 5, 10, 15, \dots$ min. The wider the window, the more flexible the cyclist will be for avoiding precipitation, or at least minimising the collected water amount. Figure 11 shows the effect of such optimisation with a fixed position at the Wettermast site. Without any flexibility, the cyclist has to start the trip exactly at 08:45 every day and will reach the destination at 09:15. In this case, the chance of getting wet (i.e., yellow or red traffic lights) is 6%. This value decreases with the increasing possibility of shifting the starting time forth and back. It is halved at slightly less than ± 30 min, meaning a starting time between 08:15 and 09:15. When considering only red trips, a flexibility of less than ± 15 min results in a halving of the original chance of getting wet. This kind of ‘half-value period’ holds also when regarding seasonal variances in precipitation types, especially in summer (typically showers) and winter (more stratiform rain events). Even though the chance of getting wet in winter

is twice the chance that it is in summer, it halves within 30 (15) min flexibility for red and yellow (red only) trips as it does in the annual view (not shown).

As an expansion of this single-point, but long-term evaluation, we now consider the spatial data of the Hamburg X-band radar with realistic cycling trips through the city, but for 2 months in summer 2020 only. Generally, the results are very similar. For the red threshold, the halve-value period is also slightly less than ± 15 min (Figure 11). When considering both yellow and red trips, the chance of getting wet without any flexibility is almost 6% as for the Wettermast but decreases faster with increasing flexibility. This results in a halve-value period of only about 15 min, which is smaller than for the Wettermast data and therefore better for the cyclist. This difference could either be only valid for this specific time period in summer but also be related to the fact that for the Wettermast analysis, we considered only trips in the morning while trips used for the X-band radar evaluation cover the whole diurnal cycle.

In any case, a precise knowledge of an upcoming precipitation event can therefore lead to substantial better conditions for cycling trips with typical durations and cyclists with a typical flexibility in time. This is not self-evident since it depends on how long the single precipitation events are and the periods between them. The precipitation interruptions must be long enough to enable a (nearly) dry trip, and the precipitation events must be short enough; otherwise, there will not be any precipitation interruptions in the considered time slot. In the spatial view, the size of precipitation cells and bands

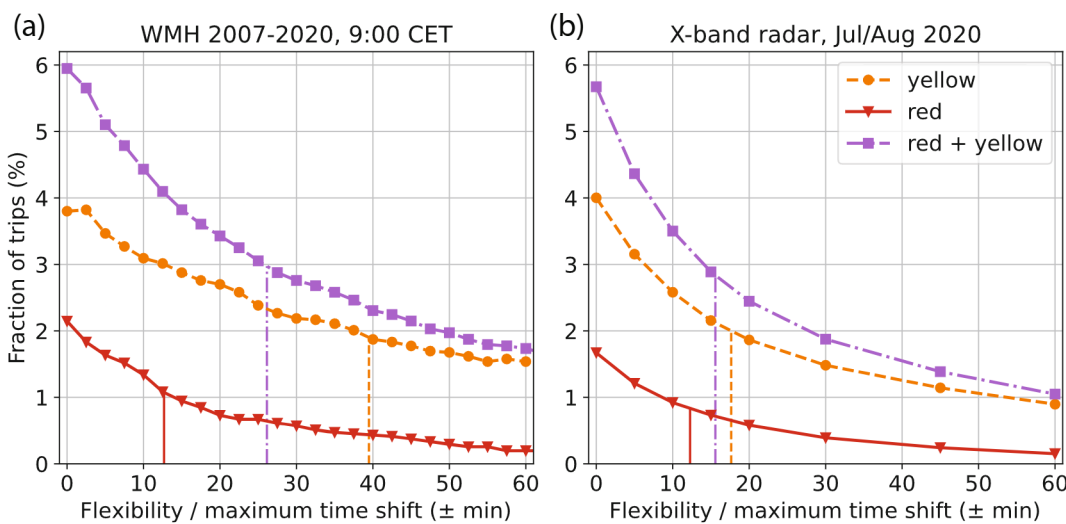


FIGURE 11 Fraction of trips classified as red and/or yellow according to the precipitation thresholds as a function of flexibility of the starting time. Panel (a) is based on Wettermast data from 2007 to 2020 assuming reference trips of 30 min with a fixed starting time at 09:00 CET. Panel (b) uses X-band radar data and the routes from the agent-based model for the study period in July and August 2020. Vertical lines denote the halve-value periods.

comes into account, too. We analysed the Wettermast data and found that most of the time, the results for the city of Hamburg indicate a sufficient time slot between two precipitation events and small enough precipitation cells to benefit from a time flexibility (not shown), which may also be valid for a greater area in Central Europe.

5.2 | Realistic forecast

Now that we know the potential of a perfect forecast, let us examine the potential of realistic forecasts. Cyclist can make use of different forecasting methods to plan their upcoming cycling trips. The simplest forecast may be persistence, that is, expecting the same weather today as yesterday. Another way of forecasting is nowcasting, that is, looking out of the window and predicting the weather at the starting point for the entire cycling trip. Lastly, numerical weather prediction (NWP) provides forecasts at least twice a day. For Hamburg, we assume that cyclists will typically consider forecasts from 12 UTC to plan their cycling trips for the next day. NWP forecasts can come with varying spatial resolution. To mimic the latter, we investigate the forecasts of the COSMO-D2 model, once with the full spatial resolution and once as a single grid cell averaged over Hamburg.

Compared with our baseline data sets based on measurements (Section 4.2), only about 20% of the critical precipitation conditions are classified correctly by NWP (Figure 12), while nowcasting exceeds this value by about 10%. In the case of wind, all forecasts are only a poor source of information about critical cycling conditions with less than 10% of trips being classified correctly. Unlike for wind conditions, all forecasts show a good skill in predicting critical temperature conditions. Around 70% of the critical temperature conditions are classified correctly by NWP and even about 80% by nowcasting.

A higher resolution of the COSMO model only offers a small but mostly marginal added value for temperature, while for precipitation and wind, the spatially averaged forecast even outperforms the full resolution forecast. As one would have expected, persistence performs best for temperature, for which more than 50% of the critical trips are classified correctly, but yields only poor results for fast-changing precipitation conditions.

So far, we neglected that there are different types of cyclists. Some cyclists are more sensitive to experiencing bad weather, and others care more about missing good weather rides, and, thus, judge their risk differently. The potential of the COSMO-D2 ensemble predictions to reduce the frustration of both cyclist types considering their individual risk perception (Goldmann & Wessel, 2020) is

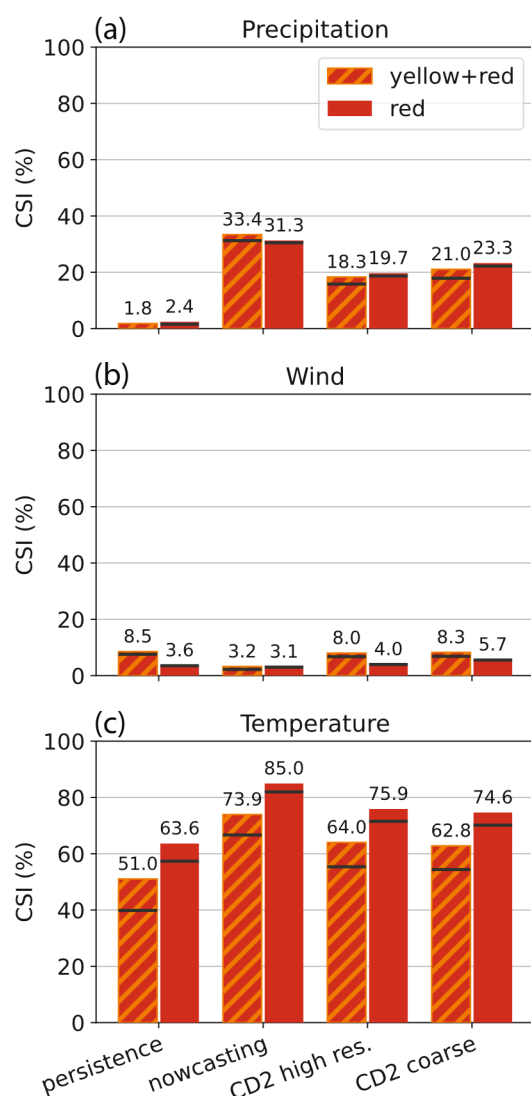


FIGURE 12 CSIs between the forecasts denoted at the *x*-axis and the corresponding baseline data sets, which are X-band radar for precipitation (a), WMH-HUSCO-WXT for wind (b), and WMH-HUSCO-WXT-APOLLO for temperature (c). Red bars consider only trips classified as red and striped bars consider both red and yellow trips. The black horizontal lines indicate the corresponding ETS values.

evaluated with the frustration reduction rate (Section 3.3.2). The added value for reducing the frustration is analysed for the main COSMO-D2 run and the ensemble by increasing the number of required ensemble members, which need to exceed the threshold to trigger a forecast for bad weather (Figure 13). To distinguish between good and bad weather conditions, yellow and red are considered one category for this analysis.

One of the most challenging parameters to forecast with numerical weather prediction is precipitation, because of the involved cloud microphysics and the small-scale structures of, for example, rain showers.

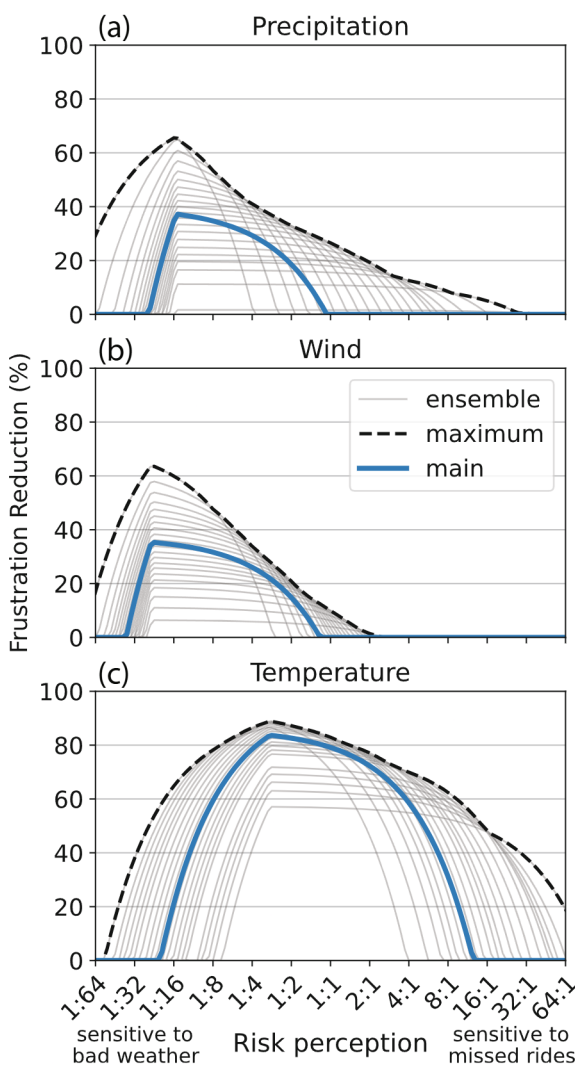


FIGURE 13 Frustration rate reduction possibilities by COSMO-D2 ensemble predictions. Main COSMO-D2 run (blue line), increasing number of ensemble members that warn (grey thin lines) and envelope of all members (black line).

Numerical weather forecasts give the highest added value for people who are sensitive to bad weather. A frustration reduction of almost 40% for the main run and of up to 68% for the ensemble can be reached (Figure 13a). Concerning wind forecasts, COSMO-D2 is most helpful for cyclists who try to avoid bad weather conditions more than missed rides and almost no added value is seen for the others. The dissatisfaction by bad wind conditions for a risk perception of 1-to-30 is reduced by up to 65% using the ensemble, which is 30% more than for the main run (Figure 13b).

Regarding temperature, for people with an approximately balanced risk perception, that is who do not want to miss a ride but also do not want to experience too hot temperatures, COSMO-D2 forecasts can help to reduce their frustration by up to 80% and even by up to 90%

using the ensemble (Figure 13c). The more sensitive the cyclists are either to bad weather or missed rides, the less value the forecasts provide. In total, the COSMO-D2 numerical weather predictions provide a substantial benefit for the route planning of cyclists to avoid bad weather or missed rides, especially in the case of temperature. For wind and precipitation, these forecasts are useful only for people who weigh the chance of avoiding uncomfortable weather higher than the harm of missing rides.

6 | SUMMARY AND CONCLUSIONS

In this study, we assess the weather conditions experienced on individual cycling routes through the urban area of Hamburg as well as how weather observations and forecasts may give guidance to a better cycling experience. To answer these two key questions, we introduce a novel agent-based model analysing a huge ensemble of randomly drawn routes that simulate cycling trips of commuters in Hamburg and assess the meteorological comfort of each ride with a three-category traffic light scheme based on thresholds for precipitation, wind and temperature.

Long-term data of 14 years from a single station show that weather conditions for cycling in Hamburg are favourable on average two-thirds of the time and cause severe discomfort only up to 10% of the time. In line with previous studies (Brandenburg et al., 2007; Goldmann & Wessel, 2020), we find that temperature is the most dominant meteorological factor causing discomfort for cyclists. Temperatures exceed favourable cycling conditions for on average one-third of the year, exhibiting a strong seasonal cycle with most discomfort (up to almost 70%) caused in winter. Remarkably, precipitation and wind lead to cycling discomfort for only about 5% of the time. Contrary to Hamburg's reputation of being a rainy and windy city, more than 90% of the time dry and windless cycling is possible in all months. Rain events cause most considerable discomfort in only 2.3% of the time, wind in only 0.2% of the time. Thus, most of the time, precipitation or wind conditions are not relevant for cyclists in climatic conditions similar to Hamburg.

Confronting the commonly used single-station approach to spatially dense observations from an urban station network and radar measurements, we find that temperature conditions can be well assessed by a single station, but only one-third of the critical precipitation events and 10% of the critical wind events are captured. Discomfort by precipitation and wind has a high spatial and temporal variability, which gives potential of guidance by weather observations to nowcast and reduce the

risk of bad weather rides. We show that with a perfect knowledge and if flexible working times may allow, the risk of getting wet can be halved by a flexible starting time of less than ± 30 min and the risk of getting severely wet by only ± 15 min.

Day-ahead forecasts by operational ensemble forecast provide almost perfect guidance in terms of temperature, but the limited predictability of precipitation and wind renders these forecasts useful only for riders with a high risk-awareness, that is, who try hard to avoid bad weather and are not very prone to missing rides. For forecasting critical precipitation conditions, nowcasting offers the greatest potential—about 30% of critical precipitation is correctly predicted this way. Numerical weather prediction correctly predicts only about 20% of the critical precipitation conditions.

In conclusion, this study indicates that weather should not be severely limiting biking commuters and highlights the potential of guidance by weather observations and forecasts to reduce the risk to experience bad weather during a ride. The results also underline the benefits of spatially dense measurements and consequently, future studies should be based on more than a single weather station. Especially when considering cycling conditions in different climate zones, it could also be relevant to include other weather parameters, such as snow or icy roads, thunderstorms or fog.

AUTHOR CONTRIBUTIONS

Amelie U. Schmitt: Conceptualization (equal); formal analysis (equal); methodology (equal); visualization (equal); writing – original draft (equal); writing – review and editing (equal). **Finn Burgemeister:** Conceptualization (equal); data curation (equal); methodology (equal); software (equal); visualization (equal); writing – original draft (equal); writing – review and editing (equal).

Henning Dorff: Conceptualization (equal); data curation (equal); formal analysis (equal); methodology (equal); visualization (equal); writing – original draft (equal); writing – review and editing (equal). **Tobias Finn:** Conceptualization (equal); methodology (equal); software (equal); writing – original draft (equal); writing – review and editing (equal). **Akio Hansen:** Conceptualization (equal); formal analysis (equal); methodology (equal); visualization (equal); writing – original draft (equal); writing – review and editing (equal). **Bastian Kirsch:** Conceptualization (equal); data curation (equal); methodology (equal); visualization (equal); writing – original draft (equal); writing – review and editing (equal).

Ingo Lange: Conceptualization (equal); data curation (equal); formal analysis (equal); methodology (equal); visualization (equal); writing – original draft (equal); writing – review and editing (equal). **Jule Radtke:** Conceptualization (equal); methodology (equal); visualization (equal); writing – original draft (equal); writing – review and editing (equal). **Felix Ament:** Conceptualization (equal); methodology (equal); visualization (equal); writing – original draft (equal); writing – review and editing (equal).

Radtke: Conceptualization (equal); methodology (equal); writing – original draft (equal); writing – review and editing (equal). **Felix Ament:** Conceptualization (equal); methodology (equal); writing – original draft (equal); writing – review and editing (equal).

ACKNOWLEDGEMENTS

This work was partly funded by the Deutsche Forschungsgemeinschaft (DFG, German Research Foundation) under Germany's Excellence Strategy—EXC 2037 'CLICCS—Climate, Climatic Change, and Society'—Project Number: 390683824, contribution to the Center for Earth System Research and Sustainability (CEN) of Universität Hamburg. The FESST@HH field experiment was carried out at the Hans Ertel Center for Weather Research (HErZ). This German research network of universities, research institutions and the German Weather Service (DWD) is funded by the Federal Ministry of Transport and Digital Infrastructure: 4818DWDP1B (BMVI). We acknowledge the DWD for providing the Consortium for Small-scale Modelling (COSMO)-D2 and C-band radar data. Open Access funding enabled and organized by Projekt DEAL.

CONFLICT OF INTEREST STATEMENT

The authors declare no conflict of interest.

DATA AVAILABILITY STATEMENT

The data that support the findings of this study are available from the authors upon reasonable request. X-band radar data are openly available in the WDC CLIMATE archive at http://doi.org/10.26050/WDCC/LAWR_UHH_HHG. Data from the APOLLO and WXT weather stations are openly available at <http://doi.org/10.25592/uhhfdm.10172>.

ORCID

Amelie U. Schmitt  <https://orcid.org/0000-0003-3346-9748>

Finn Burgemeister  <https://orcid.org/0000-0001-5144-6326>

Henning Dorff  <https://orcid.org/0000-0003-3238-1891>

Tobias Finn  <https://orcid.org/0000-0001-9585-8349>

Akio Hansen  <https://orcid.org/0000-0002-6043-1908>

Bastian Kirsch  <https://orcid.org/0000-0002-9682-0171>

Ingo Lange  <https://orcid.org/0000-0002-9561-1968>

Jule Radtke  <https://orcid.org/0000-0002-0387-5860>

Felix Ament  <https://orcid.org/0000-0003-4500-522X>

REFERENCES

- Balcan, D., Colizza, V., Gonçalves, B., Hu, H., Ramasco, J.J. & Vespignani, A. (2009) Multiscale mobility networks and the spatial spreading of infectious diseases. *Proceedings of the National Academy of Sciences of the United States of America*, 106, 5733–5738.

- National Academy of Sciences*, 106(51), 21484–21489. Available from: <https://doi.org/10.1073/pnas.0906910106>
- Baldauf, M., Förstner, J., Klink, S., Reinhardt, T., Schraff, C., Seifert, A. et al. (2016) Kurze Beschreibung des Lokal-Modells Kürzestfrist COSMO-DE (LMK) und seiner Datenbanken auf dem Datenserver des DWD. *Deutscher Wetterdienst* https://www.dwd.de/SharedDocs/downloads/DE/modelldokumentationen/nw_v/cosmo_de/cosmo_de_dbbeschr_version_2_4_161124.html
- Baldauf, M., Seifert, A., Förstner, J., Majewski, D., Raschendorfer, M. & Reinhardt, T. (2011) Operational convective-scale numerical weather prediction with the COSMO model: description and sensitivities. *Monthly Weather Review*, 139(12), 3887–3905. Available from: <https://doi.org/10.1175/MWR-D-10-05013.1>
- Bean, R., Pojani, D. & Corcoran, J. (2021) How does weather affect bikeshare use? A comparative analysis of forty cities across climate zones. *Journal of Transport Geography*, 95, 103155. Available from: <https://doi.org/10.1016/j.jtrangeo.2021.103155>
- Böcker, L. & Thorsson, S. (2014) Integrated weather effects on cycling shares, frequencies, and durations in Rotterdam, The Netherlands. *Weather, Climate, and Society*, 6(4), 468–481. Available from: <https://doi.org/10.1175/wcas-d-13-00066.1>
- Boeing, G. (2017) OSMnx: new methods for acquiring, constructing, analyzing, and visualizing complex street networks. *Computers, Environment and Urban Systems*, 65, 126–139. Available from: <https://doi.org/10.1016/j.comenvurbsys.2017.05.004>
- Brandenburg, C., Matzarakis, A. & Arnberger, A. (2007) Weather and cycling—a first approach to the effects of weather conditions on cycling. *Meteorological Applications*, 14(1), 61–67. Available from: <https://doi.org/10.1002/met.6>
- Brümmer, B., Lange, I. & Konow, H. (2012) Atmospheric boundary layer measurements at the 280 m high Hamburg weather mast 1995–2011: mean annual and diurnal cycles. *Meteorologische Zeitschrift*, 21(4), 319–335. Available from: <https://doi.org/10.1127/0941-2948/2012/0338>
- Burgemeister, F., Clemens, M. & Ament, F. (2022) Multi-year X-band weather radar observations in Hamburg (LAWR HHG). https://doi.org/10.26050/WDCC/LAWR_UHH_HHG, https://www.wdc-climate.de/ui/entry?acronym=LAWR_UHH_HHG
- Burgemeister, F., Clemens, M. & Ament, F. (2023) Reanalysis of multi-year high-resolution X-band weather radar observations in Hamburg. *Earth System Science Data Discussions*, 2023, 1–26. Available from: <https://doi.org/10.5194/essd-2023-300> <https://essd.copernicus.org/preprints/essd-2023-300/>
- de Haas, M. & Hamersma, M. (2020) *Cycling facts: new insights*. KiM Netherlands Institute for Transport. Policy Analysis <https://english.kimnet.nl/publications/publications/2020/11/03/cycling-facts-new-insights> [Accessed 9th June 2023].
- Deutscher Wetterdienst. (2022a) *Warnkriterien*. https://www.dwd.de/DE/wetter/warnungen_aktuell/kriterien/warnkriterien.html [Accessed 4th July 2022].
- Deutscher Wetterdienst. (2022b) *Wetter- und Klimalexikon*. <https://www.dwd.de/DE/service/lexikon/Functions/glossar.html?nn=103346&lv2=101812&lv3=101906> [Accessed 4th July 2022].
- Fanger, O. (1970) Thermal comfort. Analysis and applications in environmental engineering. *Royal Society of Health Journal Copenhagen: Danish Technical Press*, 92(3), 164. Available from: <https://doi.org/10.1177/146642407209200337>
- Fischereit, J. (2021) The simple urban radiation model for estimating mean radiant temperature in idealised street canyons. *Urban Climate*, 35, 100694. Available from: <https://doi.org/10.1016/j.uclim.2020.100694>
- Freie und Hansestadt Hamburg. (2018a) *Dauerzählstelle (Rad) Gurlittinsel Hamburg*. Hamburg, Germany: Behörde für Verkehr und Mobilitätswende. <https://geoportal-hamburg.de/geo-online> [Accessed 23rd November 2020].
- Freie und Hansestadt Hamburg. (2018b) *Flächennutzungsplan Hamburg*. Hamburg, Germany: Behörde für Stadtentwicklung und Wohnen. <https://metaver.de/trefferanzeige?cmd=doShowDocument&docuuid=DFDA2969-A041-433B-BD65-4CDA9F830A55> [Accessed 1st December 2020].
- Freie und Hansestadt Hamburg. (2022) *Radverkehrsmengen (Stadtradeln) Hamburg*. Hamburg, Germany: Behörde für Verkehr und Mobilitätswende. <https://metaver.de/trefferanzeige?cmd=doShowDocument&docuuid=BE8ADF33-EAE3-4F55-A913-600391A35B8C> [Accessed 8th June 2023].
- Goldmann, K. & Wessel, J. (2020) Some people feel the rain, others just get wet: an analysis of regional differences in the effects of weather on cycling. *Research in Transportation Business & Management*, 40, 100541. Available from: <https://doi.org/10.1016/j.rtbm.2020.100541>
- Heistermann, M., Jacobi, S. & Pfaff, T. (2013) Technical note: an open source library for processing weather radar data (wradlib). *Hydrology and Earth System Sciences*, 17(2), 863–871. Available from: <https://doi.org/10.5194/hess-17-863-2013>
- Helbich, M., Böcker, L. & Dijst, M. (2014) Geographic heterogeneity in cycling under various weather conditions: evidence from greater Rotterdam. *Journal of Transport Geography*, 38, 38–47. Available from: <https://doi.org/10.1016/j.jtrangeo.2014.05.009>
- Hoffmann, P., Fischereit, J., Heitmann, S., Schlünzen, K.H. & Gasser, I. (2018) Modeling exposure to heat stress with a simple urban model. *Urban Science*, 2(1), 9. Available from: <https://doi.org/10.3390/urbansci2010009>
- Jacobi, S. & Heistermann, M. (2016) Benchmarking attenuation correction procedures for six years of single-polarized C-band weather radar observations in south-West Germany. *Geomatics, Natural Hazards and Risk*, 7(6), 1785–1799. Available from: <https://doi.org/10.1080/19475705.2016.1155080>
- Jendritzky, G. (1990) Bioklimatische Bewertungsgrundlage der Räume am Beispiel von mesoskaligen Bioklimakarten. *Akad. f. Raumforschung u. Landesplanung*, 114, 7–69.
- Kirsch, B., Hohenegger, C., Klocke, D., Senke, R., Offermann, M. & Ament, F. (2021) *FESST@HH Meteorological Network Measurements*. <https://doi.org/10.25592/UHHFDM.10172>
- Kirsch, B., Hohenegger, C., Klocke, D., Senke, R., Offermann, M. & Ament, F. (2022) Sub-mesoscale observations of convective cold pools with a dense station network in Hamburg, Germany. *Earth System Science Data*, 14, 3531–3548. Available from: <https://doi.org/10.5194/essd-14-3531-2022>
- Kraemer, J.D., Zaccaro, H.N., Roffenbender, J.S., Baig, S.A., Graves, M.E., Hauler, K.J. et al. (2015) Assessing the potential for bias in direct observation of adult commuter cycling and helmet use. *Injury Prevention*, 21(1), 42–46. Available from: <https://doi.org/10.1136/injuryprev-2014-041285>
- Kraemer, P., Marro, M., Correia, H. & Salizzoni, P. (2021) Preliminary study on crosswind aerodynamics for a group of road race

- cyclists. *SN Applied Sciences*, 3(2), 279. Available from: <https://doi.org/10.1007/s42452-021-04233-z>
- de Kruijf, J., van der Waerden, P., Feng, T., Böcker, L., van Lierop, D., Ettema, D. et al. (2021) Integrated weather effects on e-cycling in daily commuting: a longitudinal evaluation of weather effects on e-cycling in The Netherlands. *Transportation Research Part A: Policy and Practice*, 148, 305–315. Available from: <https://doi.org/10.1016/j.tra.2021.04.003>
- Lengfeld, K., Clemens, M., Muenster, H. & Ament, F. (2014) Performance of high-resolution X-band weather radar networks—the PATTERN example. *Atmospheric Measurement Techniques*, 7, 4151–4166. Available from: <https://doi.org/10.5194/amt-7-4151-2014>
- Lenormand, M., Bassolas, A. & Ramasco, J.J. (2016) Systematic comparison of trip distribution laws and models. *Journal of Transport Geography*, 51, 158–169. Available from: <https://doi.org/10.1016/j.jtrangeo.2015.12.008>
- Lißner, S., Francke, A. & Becker, T. (2018) Modeling cyclists traffic volume—can bicycle planning benefit from smartphone based data? In: *Proceedings of 7th transport research arena TRA 2018*. Vienna, Austria: pp. 16–19
- Liu, C., Susilo, Y.O. & Karlström, A. (2014) Examining the impact of weather variability on non-commuters' daily activity-travel patterns in different regions of Sweden. *Journal of Transport Geography*, 39, 36–48. Available from: <https://doi.org/10.1016/j.jtrangeo.2014.06.019>
- Marshall, J., Hitschfeld, W. & Gunn, K. (1955) Advances in radar weather. In: *Advances in geophysics*, Vol. 2. New York: Elsevier, pp. 1–56.
- Meng, M., Zhang, J., Wong, Y.D. & Au, P.H. (2016) Effect of weather conditions and weather forecast on cycling travel behavior in Singapore. *International Journal of Sustainable Transportation*, 10(9), 773–780. Available from: <https://doi.org/10.1080/15568318.2016.1149646>
- Miranda-Moreno, L.F. & Nosal, T. (2011) Weather or not to cycle. *Transportation Research Record: Journal of the Transportation Research Board*, 2247(1), 42–52. Available from: <https://doi.org/10.3141/2247-06>
- Morton, C. (2020) The demand for cycle sharing: examining the links between weather conditions, air quality levels, and cycling demand for regular and casual users. *Journal of Transport Geography*, 88, 102854. Available from: <https://doi.org/10.1016/j.jtrangeo.2020.102854>
- Nankervis, M. (1999) The effect of weather and climate on bicycle commuting. *Transportation Research Part A: Policy and Practice*, 33(6), 417–431. Available from: [https://doi.org/10.1016/s0965-8564\(98\)00022-6](https://doi.org/10.1016/s0965-8564(98)00022-6)
- Nobis, C. (2019) *Mobilität in Deutschland- MiD: Analysen zum Radverkehr und Fußverkehr*. Studie von infas, DLR, IVT und infas 360 im Auftrag des Bundesministeriums für Verkehr und digitale Infrastruktur. Available from: https://www.mobilitaet-in-deutschland.de/archive/pdf/MiD2017_Analyse_zum_Rad_und_Fussverkehr.pdf [Accessed 9th June 2023].
- Nosal, T. & Miranda-Moreno, L.F. (2014) The effect of weather on the use of north American bicycle facilities: a multi-city analysis using automatic counts. *Transportation Research Part A: Policy and Practice*, 66, 213–225. Available from: <https://doi.org/10.1016/j.tra.2014.04.012>
- Richardson, D.S. (2000) Skill and relative economic value of the ECMWF ensemble prediction system. *Quarterly Journal of the Royal Meteorological Society*, 126(563), 649–667. Available from: <https://doi.org/10.1002/qj.49712656313>
- Schantz, P. (2017) Distance, duration, and velocity in cycle commuting: analyses of relations and determinants of velocity. *International Journal of Environmental Research and Public Health*, 14(10), 1166. Available from: <https://doi.org/10.3390/ijerph14101166>
- Schlichting, H.J. & Nobbe, R. (1983) Untersuchungen zur Energetik des Fahrrads. *Technic-Didact*, 8, 225–230.
- Schneider, F., Jensen, A.F., Daamen, W. & Hoogendoorn, S. (2022) Empirical analysis of cycling distances in three of Europe's most bicycle-friendly regions within an accessibility framework. *International Journal of Sustainable Transportation*, 17, 1–15. Available from: <https://doi.org/10.1080/15568318.2022.2095945>
- Statistikamt Nord. (2011) *Ergebnisse Zensus 2011 für Hamburg*. Available from: <https://www.statistik-nord.de/zahlen-fakten/zensus/ergebnisse-zensus-2011/ergebnisse-fuer-hamburg> [Accessed 1st December 2020].
- Statistikamt Nord. (2020) *Hamburger Stadtteil-Profile Berichtsjahr 2019*. Available from: <https://www.statistik-nord.de/zahlen-fakten/regionalstatistik-datenbanken-und-karten/hamburger-stadtteil-profile-staedtestatistik-fuer-hamburg> [Accessed 1st December 2020].
- Thomas, T., Jaarsma, R. & Tutert, B. (2012) Exploring temporal fluctuations of daily cycling demand on Dutch cycle paths: the influence of weather on cycling. *Transportation*, 40(1), 1–22. Available from: <https://doi.org/10.1007/s11116-012-9398-5>
- Tin Tin, S., Woodward, A., Robinson, E. & Ameratunga, S. (2012) Temporal, seasonal and weather effects on cycle volume: an ecological study. *Environmental Health*, 11, 1–9. Available from: <https://doi.org/10.1186/1476-069x-11-12>
- Wessel, J. (2020) Using weather forecasts to forecast whether bikes are used. *Transportation Research Part A: Policy and Practice*, 138, 537–559. Available from: <https://doi.org/10.1016/j.tra.2020.06.006>
- Wiesner, S. (2013) Observing the impact of soils on local urban climate (PhD thesis). University of Hamburg. Available from: <https://ediss.sub.uni-hamburg.de/handle/ediss/4942>
- Yang, L.E., Hoffmann, P., Scheffran, J., Rühe, S., Fischereit, J. & Gasser, I. (2018) An agentbased modeling framework for simulating human exposure to environmental stresses in urban areas. *Urban Science*, 2(2), 36. Available from: <https://doi.org/10.3390/urbansci2020036>
- Yang, Y., Herrera, C., Eagle, N. & González, M.C. (2014) Limits of predictability in commuting flows in the absence of data for calibration. *Scientific Reports*, 4(1), 1–9 <https://www.nature.com/articles/srep05662>.
- Zhao, J., Wang, J., Xing, Z., Luan, X. & Jiang, Y. (2018) Weather and cycling: mining big data to have an in-depth understanding of the association of weather variability with cycling on an off-road trail and an on-road bike lane. *Transportation Research Part A: Policy and Practice*, 111, 119–135. Available from: <https://doi.org/10.1016/j.tra.2018.03.001>

How to cite this article: Schmitt, A. U., Burgemeister, F., Dorff, H., Finn, T., Hansen, A., Kirsch, B., Lange, I., Radtke, J., & Ament, F. (2023). Assessing the weather conditions for urban cyclists by spatially dense measurements with an agent-based approach. *Meteorological Applications*, 30(6), e2164. <https://doi.org/10.1002/met.2164>